JOURNAL OF VIROLOGY, Dec. 2011, p. 12376–12386 Vol. 85, No. 23
0022-538X/11/$12.00 doi:10.1128/JVI.00016-11

Decay-Accelerating Factor Binding Determines the Entry Route of Echovirus 11 in Polarized Epithelial Cells[▽]

Komla Sobo,[1,2,3]* Laura Rubbia-Brandt,[1] T. David K. Brown,[3] Amanda D. Stuart,[3] and Thomas A. McKee[1]

Department of Clinical Pathology, University of Geneva, 1 Rue Michel Servet, 1211 Geneva 4, Switzerland[1]; Cell Biology Unit, MRC Laboratory for Molecular Cell Biology, University College London, Gower Street, London WC1E 6BT, United Kingdom[2]; and Division of Virology, Department of Pathology, University of Cambridge, Tennis Court Road, Cambridge CB2 1QP, United Kingdom[3]

Received 4 January 2011/Accepted 4 September 2011

The interaction between echovirus 11 strain 207 (EV11-207) and decay-accelerating factor (DAF or CD55) at the apical surface of polarized Caco-2 cells results in rapid transport of the virus to tight junctions and in its subsequent uptake. A virus mutant (EV11-207R) which differs at 6 amino acids and whose affinity for DAF is apparently significantly lower remains at the apical surface, from where its uptake occurs. Binding of EV11-207 to DAF and its transport to tight junctions result in a loss of function of the junctions. In contrast, the mutant virus EV11-207R is not transferred to tight junctions, nor does it impair the integrity of these junctions. Cholesterol depletion from the apical membrane leads to DAF aggregation and, presumably, internalization and inhibits infection by EV11-207. However, infection by EV11-207R is significantly less sensitive to cholesterol depletion than infection by EV11-207, confirming the DAF requirement for EV11-207, but not EV11-207R, to infect cells. These data strongly indicate that in the case of infection of polarized epithelial cells by echovirus 11, DAF binding appears be a key determinant in the choice of entry pathway, at least in cell culture.

Many viruses initiate infection at respiratory or intestinal epithelial surfaces (8, 10, 13, 14, 20, 41, 42, 44, 53). These surfaces are lined by polarized epithelial cells that are connected by a variety of specialized cell-cell contacts to form a barrier that separates the inside of the organism from its environment. Key to the formation of this barrier are tight junctions. These are macromolecular complexes formed by intercellular interactions of claudins, occludin, and junction-adhesion molecules (JAMs) with associated scaffolding proteins, such as ZO-1 (7, 9, 19, 21, 23, 30, 45). At the tissue level, tight junctions regulate the paracellular passage of proteins and other molecules and thus maintain a barrier between the body and the external environment that in many cases must be breached by microorganisms in order to establish infections. At the cellular level, tight junctions separate the plasma membrane into two domains. These apical and basolateral domains have different protein and lipid compositions. Tight junctions are known to be dynamic structures with a baseline protein turnover that varies for the different protein components (22, 43, 50).

The echoviruses (enteric cytopathic human orphan viruses), a group of human virus isolates that cannot be grown in suckling mice, are grouped with coxsackie B viruses (CVB) to form the human enterovirus B species within the *Enterovirus* genus of the family *Picornaviridae*. While most echovirus infections are asymptomatic or cause only mild symptoms, they can also result in meningitis, encephalitis, myocarditis, hemorrhagic conjunctivitis, and severe generalized neonatal infections. However, these syndromes are not associated with specific serotypes (47).

We have studied a strain of echovirus 11 (EV11) isolated directly from human colon epithelial cells (EV11-207) during an outbreak of diarrhea (36). We showed that this virus, like several other enteroviruses, binds to the glycosylphosphatidylinositol (GPI)-anchored cell surface protein decay-accelerating factor (DAF; also called CD55) (29, 46). This protein was shown to be necessary for virus entry, but purified DAF failed to induce the conformational changes in EV7 and EV11 capsids that are thought to be crucial for virus uncoating (39; our own observations). The interaction between DAF and virus was characterized by a low affinity (in the micromolar range) and high on and off rates compared with enterovirus receptors capable of causing a conformational change to the capsid (29, 46, 47). Passage of EV11-207 in nonpermissive Vero cells followed by repassage in HT29 cells resulted in a virus mutant (EV11-207R) differing in 6 amino acids from the wild type. These changes apparently resulted in a significant decrease in the affinity of the DAF-virus interaction (29). When the entry pathways of these viruses were compared in nonpolarized epithelial cells, EV11-207 entry proved to be dependent on lipid rafts, the actin cytoskeleton, and microtubules. In contrast, entry of EV11-207R was sensitive only to interference with the formation of clathrin-coated pits (29, 46, 47).

Recently, it was shown that binding of coxsackievirus B3 (CVB3) to DAF at the apical surface of epithelial cells results in transfer of virus to the tight junctions, followed by internalization of both virus and tight junction proteins (10, 12). Moreover, cryo-electron microscopy studies have shown that the interaction between DAF and echoviruses differs significantly

* Corresponding author. Mailing address: Department of Pathology, Virology Division, University of Cambridge, Tennis Court Road, Cambridge CB2 1QP, United Kingdom. Phone: (44) 012 2333 6918. Fax: (44) 012 2333 6926. E-mail: ks607@cam.ac.uk.

▽ Published ahead of print on 14 September 2011.

from the DAF-coxsackievirus interaction, to the extent that convergent evolution was invoked to explain these differences (37, 38). We therefore investigated differences in polarized epithelial cell entry between EV11-207 and EV11-207R. We found that the DAF-binding strain EV11-207 was transferred rapidly with DAF from the apical surface to tight junctions prior to the uptake of viral particles. Subsequently, the integrity of the junctions was impaired. In contrast, EV11-207R (a virus that binds DAF with an apparently lower affinity) was not transferred to tight junctions, nor did it lead to impairment of the integrity of the junctions. However, infection appeared to proceed directly from the apical surface. Infection by EV11-207 was significantly inhibited by cholesterol depletion using methyl-β-cyclodextrin (MβCD), while this drug had only a minor inhibitory effect on infection by EV11-207R. Finally, we demonstrated that cholesterol depletion led to DAF aggregation at the cell surface and to its internalization.

MATERIALS AND METHODS

Cells. Caco-2 cells, a human colon adenocarcinoma cell line (American Type Culture Collection [ATCC]), were cultured as monolayers on filters. Cells were seeded in 6.5-mm Transwell-COL inserts (0.4-μm pore size; Costar) at a density of 6×10^4 cells/cm^2 and were refed every second day. The cells were maintained in high-glucose Dulbecco's modified Eagle's medium (DMEM) containing 10% fetal calf serum and penicillin-streptomycin at 37°C and 5% CO_2. Monolayers were used between 8 and 12 days postseeding. Transepithelial electrical resistance (R_T) was measured across monolayers by use of an EVOM ohmmeter (World Precision Instruments). Confluent monolayers consistently displaying a high R_T (>300 Ω/cm^2) were used in experiments. HT29 cells were obtained from the European Collection of Cell Culture and maintained in RPMI medium as described previously (46). CHO-DAF cells were a gift from Nicolas Levêque, Centre Hospitalier Universitaire de Reims, France. They were maintained in DMEM as described elsewhere (40).

Viruses. The EV11 isolate EV11-207 and the EV11-207R mutant have been described elsewhere (46). Briefly, EV11-207 was isolated on HT29 cells from a clinical sample as previously described (36). EV11-207R was derived by passage in nonpermissive Vero cells and subsequent passage in HT29 cells (47). Stocks of both viruses were produced in HT29 cells. Confluent HT29 monolayers were infected with EV11-207 or EV11-207R at 10 PFU/cell. Infection was allowed to proceed overnight at 37°C. Cells were scraped into the culture medium, which was then subjected to freezing and thawing three times, followed by centrifugation at 2,000 × *g* for 5 min. The supernatant was harvested, and titers were determined by plaque assay on HT29 cells.

Antibodies. Primary antibodies included previously described rabbit polyclonal anti-EV11-207 and rabbit polyclonal anti-DAF antibodies (46), mouse anti-DAF (Gene Tex, Inc.), mouse anti-enterovirus (U.S. Biologicals), and mouse anti-occludin and anti-ZO-1 antibodies (both from Zymed). The secondary antibodies for immunofluorescence, i.e., tetramethyl rhodamine isocyanate (TRITC)-, fluorescein isothiocyanate (FITC)-, and Cy5-labeled goat anti-rabbit and anti-mouse antibodies, were from Jackson ImmunoResearch. Secondary antibodies conjugated to horseradish peroxidase (HRP) for Western blot analysis were obtained from Dako, Ltd., and included goat anti-rabbit and anti-mouse HRP conjugates.

Time course of EV11 infection. Between 8 and 12 days postseeding, the cells were infected with either EV11-207 or EV11-207R at 100 PFU/cell, unless stated otherwise. The infected cells were incubated at 4°C for 30 min to allow virus attachment and then washed three times with phosphate-buffered saline (PBS) before incubation at 37°C to initiate virus entry. At different time points, the cells were washed twice with PBS containing 1% newborn calf serum (PBS-NCS) and fixed with PBS containing 4% paraformaldehyde (PBS-PFA) for 10 min at room temperature (RT). The cells were then prepared for immunofluorescence analysis as described below.

Immunofluorescence analysis. Fixed cells were permeabilized with 0.05% Triton X-100 in PBS and incubated at RT for 2 min before being washed three times with PBS-NCS. Cells were incubated with the indicated primary antibodies for 45 min at RT, washed three times with PBS-NCS, incubated with fluorochrome-conjugated secondary antibodies for 30 min at RT, washed three times with PBS-NCS, incubated with 4′,6-diamidino-2-phenylindole (DAPI) for 5 min, washed three times, and mounted onto glass slides. Images were acquired in multiple sections (0.5 μm/section) from the apical pole to the basal pole, using a confocal laser scanning microscope (LSM 510 Meta; Zeiss), and were analyzed by Imaris software. All images are three-dimensional projections from the multisection scannings. *xy* and *xz* images show top and side views, respectively.

Image acquisition and colocalization quantification. Confocal images were acquired on a Zeiss LSM 510 Meta microscope. The exposure settings (appropriate values for the size of the microscope pinhole and the gain of the laser) were maintained throughout image acquisition to allow direct comparisons among images. To minimize the bleed-through effect and to avoid the loss of image data needed for quantification, images were acquired using only sequential scanning and were saved in TIFF graphic file format (56). Prior to performing measurements of colocalization, the background was suppressed by use of median filters (28). Colocalization was estimated by using an overlap coefficient (% of DAF or EV11-207 colocalizing with occludin; obtained with Imaris bitplane software) according to the method of Manders et al. (33, 56).

Paracellular permeability. Transepithelial electrical resistance (R_T) was measured using an EVOM ohmmeter (World Precision Instruments) on cell monolayers grown on Transwell-COL inserts. Confluent monolayers displayed high R_T values (>300 Ω/cm^2). The apical-to-basolateral flux of radiolabeled probes was measured to determine paracellular permeability of Caco-2 monolayers. Flux of [^{3}H]mannitol (182 Da; Sigma) and [^{14}C]dextran (10 kDa and 2,000 kDa; Sigma) was measured for 1 h at 37°C following virus binding at 4°C (30 min) as described previously (10). Briefly, [^{3}H]mannitol (5 μCi) and [^{14}C]dextran (5 μCi) were added to the apical compartment ($t = 0$), and samples (medium; 10 μl) were removed from the basolateral compartment after 1 h at 37°C. Radioactivity in each sample was counted, and the apparent permeability coefficient was calculated (10, 32, 48).

Immunoblotting and protein quantification. Proteins were separated by SDS-PAGE using 10% acrylamide gels, unless stated otherwise, and were transferred to polyvinylidene difluoride (PVDF) membranes. Western blots were revealed by use of an Amersham ECL Western blotting system (Amersham) and were quantified by densitometry.

MβCD treatments. Caco-2 cells were treated with different concentrations of MβCD (Sigma) as described previously (1, 2). Briefly, after 1 h of treatment at 37°C, MβCD was removed. The monolayers were then washed with PBS and exposed or not exposed to viruses.

RESULTS

DAF mediates infection of polarized Caco-2 cells by EV11-207 but not by EV11-207R. Our previous studies with nonpolarized cells indicated that DAF was required for binding and infection by EV11-207 but not by EV11-207R (46, 47). We sought to determine whether the same requirement for DAF existed in polarized Caco-2 cells. We found that infection of Caco-2 monolayers exposed to EV11-207 at a PFU/cell ratio of 5 showed an 18-fold reduction in infection when cells were treated with a mouse monoclonal antibody (MAb) against DAF. The same treatment of monolayers infected by EV11-207R resulted in a <2-fold reduction in infection (Fig. 1A). Moreover, we found that binding of EV11-207, but not EV11-207R, to CHO cells was dependent on DAF expression (Fig. 1B). Calculation of colocalization using overlap coefficients according to the method of Manders et al. (33, 56) allowed us to estimate that more than 80% of EV11-207 colocalized with DAF, whereas only a minority (ca. 10%) of EV11-207R colocalized with DAF (Fig. 1C).

Inhibition of infection. Our previous work (46) demonstrated the sensitivity of EV11-207 infection to drugs that interfere with membrane cholesterol in nonpolarized cells. To confirm this observation in polarized cells, Caco-2 cells were cultured as monolayers on polyester filters for differentiation. Cells were seeded in 6.5-mm Transwell-COL inserts (0.4-μm pore size) at a density of 6×10^4 cells/cm^2 and were refed every second day. Confluent monolayers (be-

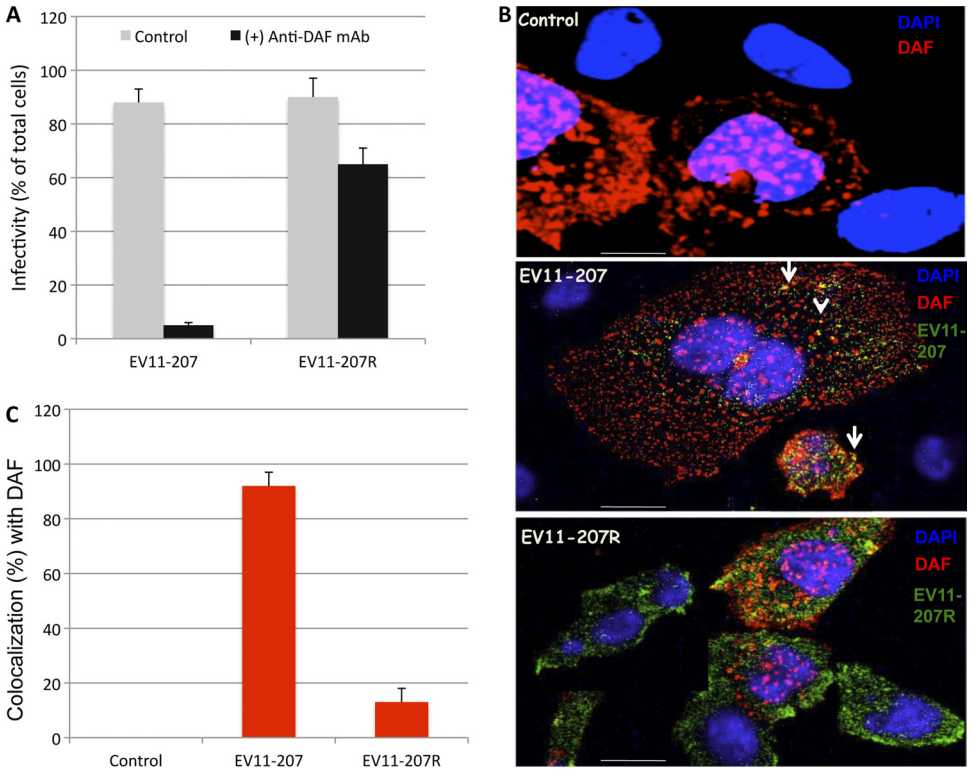

FIG. 1. EV11-207 but not EV11-207R requires DAF for binding and infection. (A) Polarized Caco-2 monolayers were exposed to anti-DAF MAb at 4°C for 1 h. The monolayers were washed and exposed to EV11-207 or EV11-207R (5 PFU/cell) at 4°C for 30 min to allow virus attachment. The cells were then washed and warmed to 37°C for 6 h. Fixed, permeabilized cells were stained with anti-EV11-207 PAb and DAPI. Cells that displayed diffuse cytoplasmic staining of EV11-207 or EV11-207R were considered infected. Infectivity is expressed as the percentage of infected cells among the total cells. Data are means plus standard deviations (SD) for 3 monolayers. (B) CHO-DAF cells were exposed to EV11-207 or EV11-207R (5 PFU/cell) at 4°C for 30 min to allow virus attachment. The cells were then washed. Fixed, permeabilized cells were stained with anti-enterovirus MAb (green), anti-DAF PAb (red), and DAPI (blue). Bars = 10 μm. (C) Colocalization of EV11-207 and EV11-207R with DAF was calculated.

tween 8 and 12 days postseeding) that consistently displayed a high R_T (>300 Ω/cm^2) and functional tight junctions (25, 34) were used in experiments. Monolayers were treated from the apical surface with 5 mM MβCD, which depletes the cell of cholesterol (1, 2, 27). After 1 h of treatment at 37°C, MβCD was removed and cells were exposed to EV11-207 or EV11-207R, using PFU/cell ratios of 1, 5, 10, 50, and 100. The results in Fig. 2E show significant reductions (≥50%) of infection by EV11-207 in Caco-2 cells, depending on the PFU/cell ratio. However, the concentration of MβCD used here did not show a significant inhibitory effect on infection by EV11-207R, with no effect at all when a PFU/cell ratio of 100 was applied.

Concomitant with inhibition of infection by EV11-207, we observed a significant decrease in viral particle binding to cells exposed to MβCD (Fig. 2A and B). Quantification of the apical membrane-bound viruses by means of fluorescence intensity (Fig. 2C) showed a 5-fold reduction for cells exposed to MβCD compared to untreated cells. Moreover, Western blotting of VP1 in untreated cells, either in cell total extract (CE) or DAF immunoprecipitation (DAF IP) samples, showed 3.5- and 4-fold higher densities, respectively, than that in MβCD-treated cells, whereas the total amount of cellular DAF did not change.

Cholesterol depletion leads to DAF aggregation and internalization. The above data raised the possibility that MβCD treatment led to mislocalization of DAF and/or interfered with the binding of EV11-207 particles to DAF. In order to examine this, we investigated the DAF distribution after MβCD treatment by immunofluorescence assay, using either nonpermeabilized or permeabilized cells. As shown in Fig. 3B, MβCD treatment led to aggregation of DAF at the cell surface and presumably to its uptake to a perinuclear localization (Fig. 3A). It might also be possible that MβCD treatment affects DAF trafficking to the plasma membrane. The absence of DAF aggregates at the cell surface in permeabilized cells (Fig. 3A) was presumably due to their depletion from the membrane during the permeabilization step (0.05% Triton X-100 for 2 min at RT).

Together, these data confirmed unambiguously the requirement of DAF for EV11-207, but not EV11-207R, to infect cells. In this context, it would be useful to determine the binding affinity and kinetic constants for interaction between EV11-207R and DAF. This is problematic at the moment, as EV11-207R aggregates during purification and therefore is not easily purified.

Time course of internalization of EV11-207 and EV11-207R. To track the entry of EV11-207 and EV11-207R into polarized

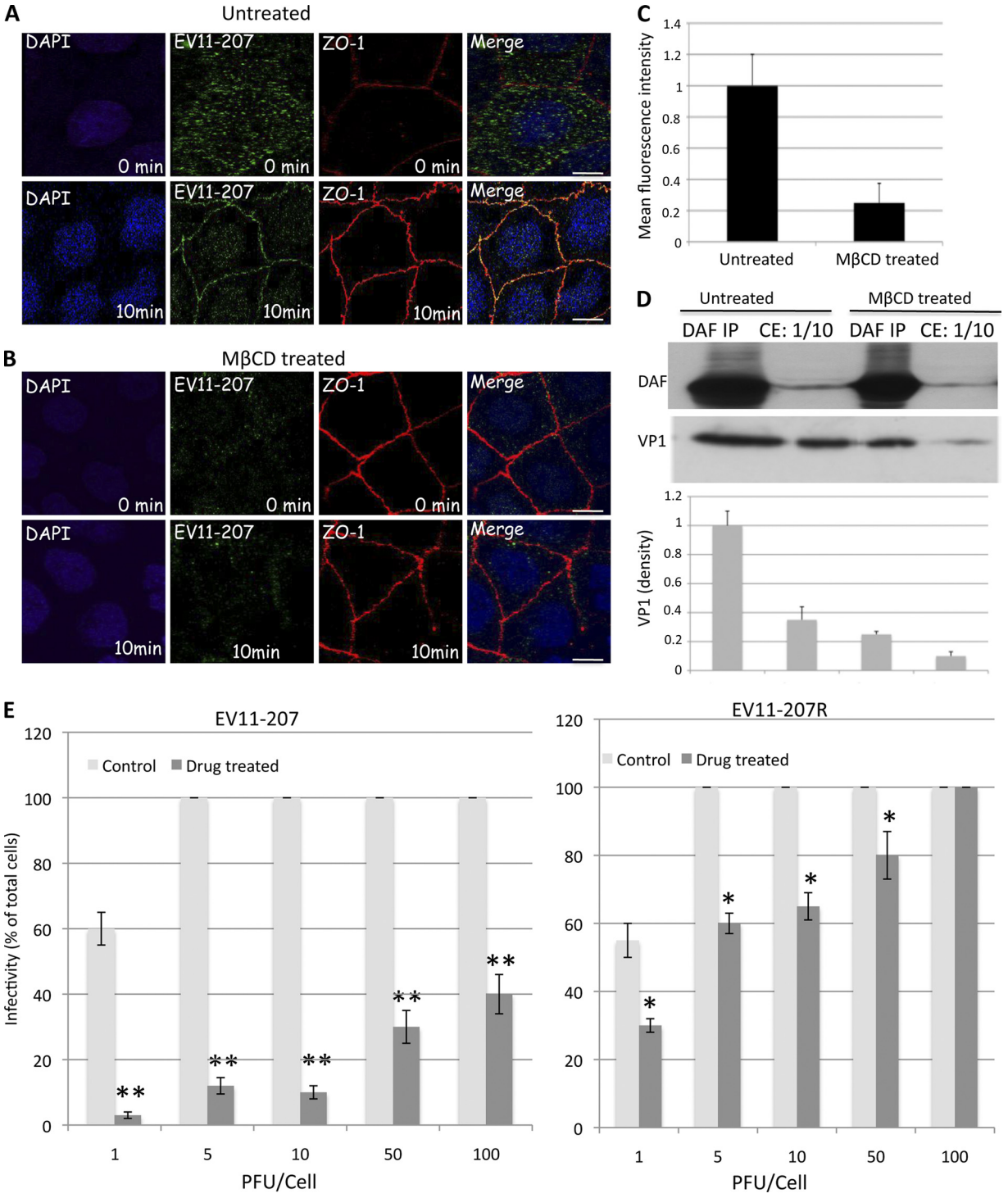

FIG. 2. MβCD (5 mM) inhibits infection by EV11-207 in a PFU-dependent manner. Polarized Caco-2 monolayers grown on Transwell membranes were left untreated (A) or treated with 5 mM MβCD (B) and then were exposed to EV11-207 (10 PFU/cell) at 4°C for 30 min to allow virus attachment. The cells were then washed (0 min) and warmed to 37°C for 10 min. Fixed, permeabilized cells were stained with anti-ZO-1 MAb (red), anti-EV11-207 PAb (green), and DAPI (blue). Bars = 10 μm. (C) Quantification of EV11-207 (10 PFU/cell) binding to MβCD-treated or untreated monolayers by means of fluorescence intensity. Data are means plus SD for 4 monolayers. (D) Western blotting of DAF and VP1. Polarized Caco-2 monolayers grown on Transwell membranes were left untreated or treated with 5 mM MβCD and then were exposed to EV11-207 (10 PFU/cell) at 4°C for 30 min to allow virus attachment. The cells were washed to remove unbound particles and lysed in NP-40 buffer (10 mM HEPES, 1.5 mM $MgCl_2$, 10 mM KCl, 0.5 mM dithiothreitol, 0.05% NP-40, pH 7.9) to prepare total cell extract (CE). One hundred microliters of CE was used for DAF immunoprecipitation (DAF IP). DAF (top) and VP1 (bottom) were analyzed by Western blotting of both CE (10 μl) and DAF IP samples. The graphic at the bottom shows the relative band intensities quantified by densitometry of the VP1 bands. Data are means plus SD for 3 monolayers. (E) Caco-2 monolayers grown on Transwell membranes were left untreated (control) or treated with 5 mM MβCD (drug treated) for 1 h at 37°C before being exposed to different amounts (PFU/cell) of EV11-207 or EV11-207R at 4°C for 30 min to allow virus attachment. The cells were washed and warmed to 37°C for 6 h. Fixed, permeabilized cells were stained with anti-EV11-207 PAb and DAPI. Infected cells that displayed diffuse cytoplasmic staining for EV11-207 were counted. Infectivity is shown as the percentage of infected cells. Data show means plus SD for 4 monolayers. *, $P < 0.005$; **, $P < 0.001$ (paired, two-tailed t test).

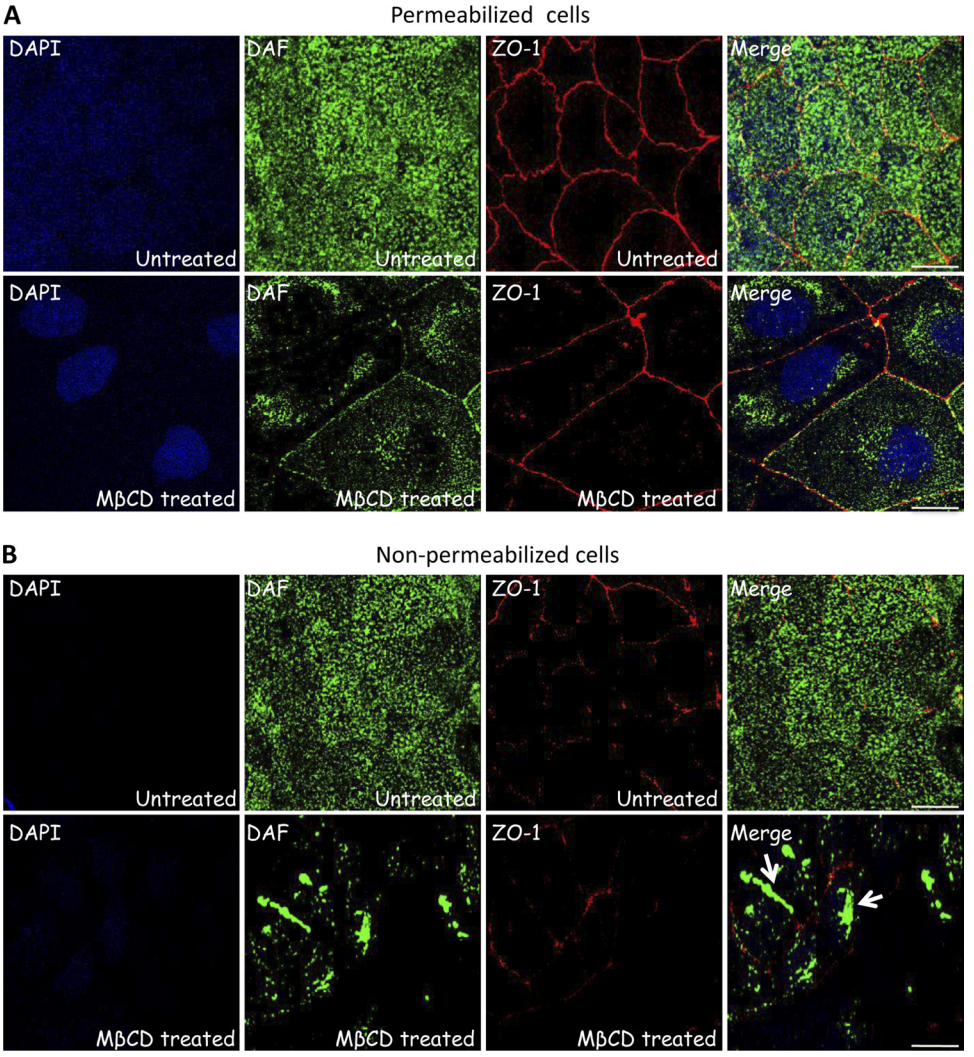

FIG. 3. MβCD treatment leads to DAF aggregation and internalization. Polarized Caco-2 monolayers grown on Transwell membranes were left untreated or treated with 5 mM MβCD at 37°C for 1 h. Cells were then fixed. Nonpermeabilized cells (B) or permeabilized cells (A) were stained with anti-ZO-1 MAb (red), anti-DAF PAb (green), and DAPI (blue). Bars = 10 μm.

Caco-2 cells, the apical surface was exposed to 100 PFU/cell of each virus for 30 min at 4°C to allow virus attachment ($t = 0$). The monolayers were then shifted to 37°C to initiate entry, which was monitored by immunofluorescence and confocal microscopy. Ten and 30 min following viral attachment, fixed permeabilized monolayers were stained with antibodies against ZO-1 and EV11 and counterstained with DAPI. Initially ($t = 0$), both viruses showed a diffuse staining pattern at the apical surface of the cells (Fig. 4A). Following warming to 37°C, EV11-207 was transferred to tight junctions, where a clear colocalization with ZO-1 (Fig. 2A and 4B) and occludin (see Fig. 7B) could be detected within 10 min. In contrast, EV11-207R was not found in tight junctions at 10 min postbinding but remained bound in a diffuse pattern on the apical surface of the cells (Fig. 4B).

At 30 min postbinding, EV11-207 was seen in structures surrounding the nucleus, and no further association with tight junctions, marked by ZO-1 (Fig. 4C) and occludin (see Fig. 7C), could be detected. At 30 min postbinding, EV11-207R, like EV11-207, was detected in perinuclear structures (Fig. 4C).

DAF cointernalizes with EV11-207 particles. Given that EV11-207 but not EV11-207R has been shown to require DAF to infect polarized epithelial cells, we specifically investigated the fate of DAF during the uptake of EV11-207 and EV11-207R. Coimmunostaining experiments were performed in which DAF and EV11-207 in fixed, permeabilized cells were stained with polyclonal antibody (PAb) and MAb, respectively. Confocal microscopy (Fig. 5) revealed that the virus and DAF colocalized at the apical surface at time zero and in the tight junctions at 10 min postbinding. Importantly, EV11-207 particles and DAF colocalized in the perinuclear region within 30 min (Fig. 5), indicating that DAF was cointernalized with EV11-207. In contrast, no significant colocalization of EV11-207R and DAF was seen from the initial step ($t = 0$) to internalization, when the EV11-207R particles were seen in the perinuclear region (Fig. 6).

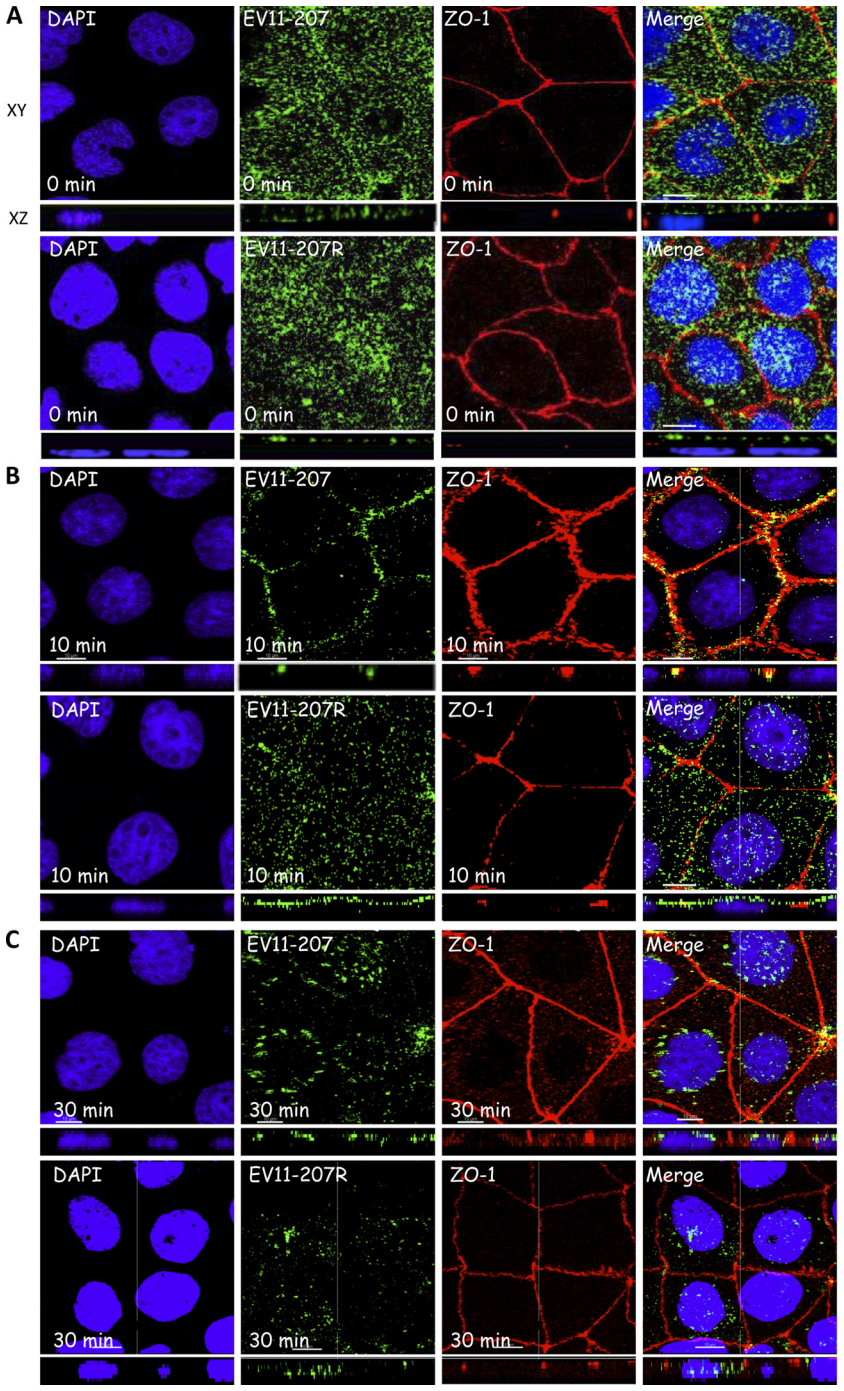

FIG. 4. EV11-207 and EV11-207R entry pathways. Polarized Caco-2 monolayers were exposed to EV11-207 or EV11-207R (100 PFU/cell) at 4°C for 30 min to allow virus attachment. The cells were then washed ($t = 0$) and warmed to 37°C. Fixed, permeabilized cells were stained with anti-ZO-1 MAb (red), anti-EV11-207 PAb (green), and DAPI (blue). (A) Both viruses showed a diffuse distribution at the apical surface. (B) At 10 min postbinding (after the warming step), EV11-207 (green) but not EV11-207R (green) colocalized with ZO-1 (red) in the tight junctions. Areas of colocalization appear yellow in the merge panels. (C) At 30 min postbinding, both EV11-207 and EV11-207R were internalized and seen concentrated in the perinuclear region. Bars = 10 μm.

These data were confirmed by quantifying the colocalization of EV11-207 and DAF with the tight junction protein occludin (Fig. 7C). Infections were performed as described above, and at 0, 10, and 30 min postinfection, immunofluorescence staining was performed and the colocalization between DAF and occludin and between EV11-207 and occludin was quantified as described in Materials and Methods. As seen in steady-state polarized Caco-2 cells, a minority of DAF was found colocalized with occludin. Addition of virus did not change this distribution significantly; in addition, only a very small proportion

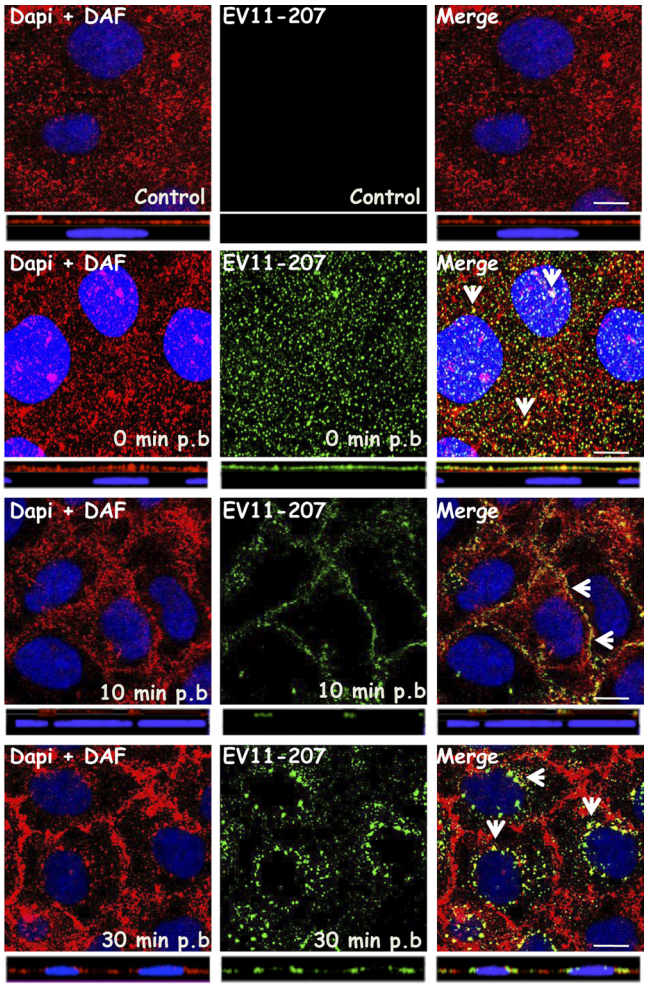

FIG. 5. EV11-207 colocalizes with DAF. Polarized Caco-2 monolayers were fixed (control) or exposed to EV11-207 (100 PFU/cell) at 4°C for 30 min to allow virus attachment. The cells were washed, warmed to 37°C for 10 or 30 min, and then fixed. Cells were permeabilized and stained with anti-enterovirus MAb (green), anti-DAF PAb (red), and DAPI (blue). Initially (t = 0), EV11-207 particles colocalized with DAF at the cell surface. At 10 min postbinding, EV11-207 colocalized with DAF in the cell-cell contacts. At 30 min postbinding, EV11-207 appeared in intracellular puncta that colocalized with DAF. Bars = 10 μm. Arrows show areas of colocalization. p.b., postbinding.

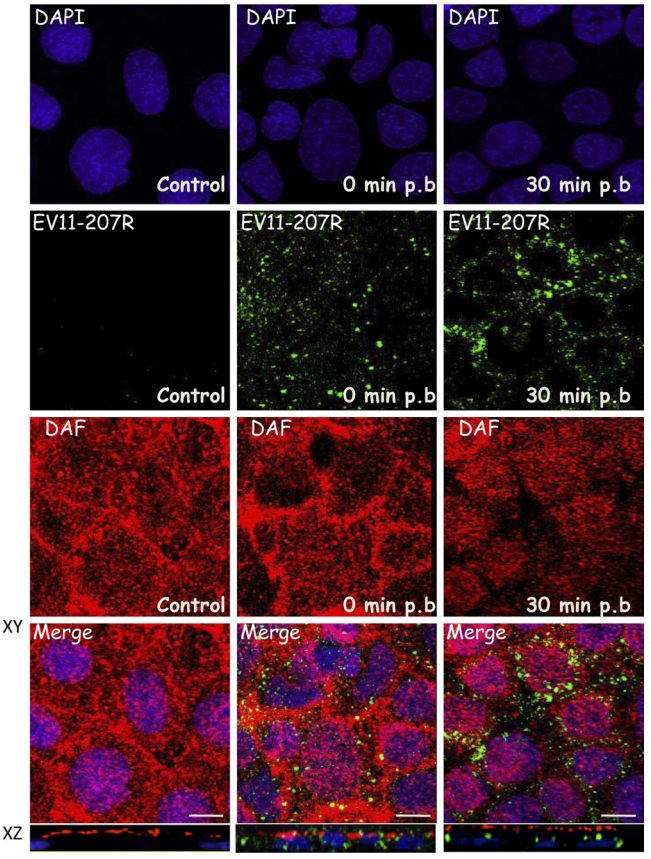

FIG. 6. EV11-207R does not colocalize with DAF. Polarized Caco-2 monolayers were fixed (control) or exposed to EV11-207R (100 PFU/cell) at 4°C for 30 min to allow virus attachment. The cells were washed, warmed to 37°C for 30 min, and then fixed. Cells were permeabilized and stained with anti-enterovirus MAb (green), anti-DAF PAb (red), and DAPI (blue). Initially (t = 0), EV11-207R particles did not colocalize significantly with DAF at the cell surface. At 30 min postbinding, EV11-207R appeared in intracellular puncta with no evident colocalization with DAF. Bars = 10 μm.

of the virus was found colocalized with occludin at the end of the binding period. Incubation at 37°C for 10 min resulted in the transfer of the vast majority of virus to the tight junction, as defined by colocalization with occludin, and this correlated with the presence of 48% of stained DAF in the same location. At the 30-min time point, the level of colocalization between DAF and occludin had fallen almost to preinfection levels, and colocalization between the virus and occludin had fallen almost to the level found at 0 min.

EV11-207 entry leads to impairment of tight junctions. The finding that EV11-207 appeared to enter polarized epithelial Caco-2 cells via tight junctions, while EV11-207R entered directly at the apical surface, led us to investigate whether tight junction integrity was affected during infection by these two viruses. As described in Materials and Methods, the transepithelial electrical resistance (R_T) was measured during infection by EV11-207 or EV11-207R. Within 10 min of the initiation of infection with EV11-207, R_T was reduced by 50% (Fig. 8A), but it recovered thereafter during the next 4 h, to nearly 80% of the control value. At 6 h, when new viruses were being produced, there was a large reduction in R_T. Infection with EV11-207R initially resulted in only a minor reduction of R_T, which remained relatively constant, at around 80% of the control value, until 6 h, when a large reduction similar to that observed with EV11-207 was seen.

To investigate whether the impermeability of tight junctions to larger molecules was compromised, we followed the flux of [^{3}H]dextran and [^{14}C]mannitol across Caco-2 monolayers (10) for 1 h as described in Materials and Methods. Results are expressed as apparent permeability coefficients (10, 32, 34, 48) and displayed in Fig. 8B, and they show evidence of increases of diffusion of 1.5- and 3.0-fold for dextran (10 kDa) and mannitol, respectively, after infection with EV11-207, suggesting that the tight junctions became more permeable to these compounds. In contrast, infection with EV11-207R resulted in no significant change in the paracellular permeability, in keep-

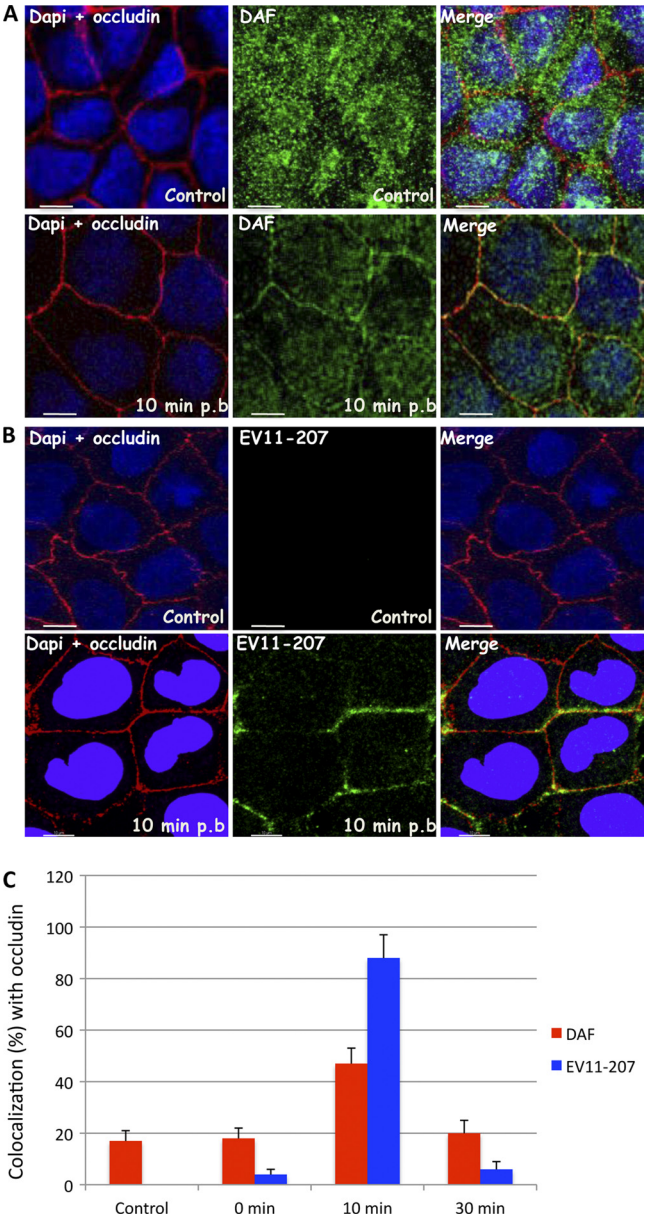

FIG. 7. EV11-207 and DAF colocalize with occludin. Polarized Caco-2 monolayers were fixed (control) or exposed to EV11-207 (100 PFU/cell) at 4°C for 30 min to allow virus attachment. The cells were washed, warmed to 37°C for 10 min, and then fixed. (A) Cells were permeabilized and stained with anti-occludin MAb (red), anti-DAF PAb (green), and DAPI (blue). At 10 min postbinding, DAF (green) colocalized with occludin (red). (B) Permeabilized cells were stained with anti-EV11-207 PAb (green), anti-occludin MAb (red), and DAPI (blue). At 10 min postbinding, EV11-207 (green) colocalized with occludin (red). (C) Percentages of DAF (red) and EV11-207 (blue) colocalizing with occludin at different postbinding steps. Data are means plus SD for 5 monolayers. Bars = 10 μm.

ing with the absence of interaction with tight junctions. There was no change in the flux of dextran (2,000 kDa) during infection with either virus, indicating that during infection by EV11-207, the tight junctions became leaky rather than totally open.

Several different types of stimuli (e.g., cytokines such as tumor necrosis factor or gamma interferon and the bacterial virulence factor lymphostatin) are known to reduce transepithelial resistance. Previous studies have demonstrated that these stimuli induce a concomitant movement of tight junction proteins from the junctions into intracellular vesicles (4, 18, 22, 23, 51, 54). Interestingly, we observed a displacement of the tight junction proteins claudin-1 and occludin (Fig. 8C) out of the junction boundary concomitant with the uptake of EV11-207 particles. However, in contrast to observations made with coxsackie B virus (12), no intracellular colocalization of EV11-207 with occludin could be detected.

DISCUSSION

The six amino acid changes that differentiate EV11-207 from EV11-207R result in major differences in the mechanisms by which these viruses enter cells. Structural data indicate that these mutations map to the surface of the enterovirus particles, around the canyon region where virus-receptor interactions have been shown to occur in other enteroviruses (47). EV11-207 has an affinity for DAF/CD55 in the micromolar range and displays high on and off rates by surface plasmon resonance analysis, while we have demonstrated here that DAF/CD55 binding by EV11-207R is undetectable on Caco-2 monolayers (Fig. 6), at least by immunofluorescence, confirming previous observations using hemagglutination inhibition and blocking of binding with anti-DAF antibodies (29). EV11-207 uses an entry pathway that depends on lipid rafts, intact actin microfilaments, and intact microtubules, as demonstrated by its sensitivity to nystatin, cytochalasin D, and nocodazole, respectively. Entry of EV11-207R was found to be less dependent on lipid rafts, actin microfilaments, and microtubules, but its entry was blocked by chlorpromazine at concentrations that affect endocytosis through clathrin-coated pits (29, 46, 47). The experiments reported here extend these observations to a polarized human intestinal cell line.

Both viruses initiate entry via the apical surface, suggesting that both attachment receptors must be located there, but with respect to the entry pathway, the similarities end there. EV11-207 transits rapidly to tight junctions prior to internalization. The transfer of EV11-207 to the tight junctions results in a transient reduction in transepithelial resistance, suggesting that the interaction of the virus particle with the tight junctions results in a partial and temporary reorganization of these structures. Thus, the initial phase of EV11-207 entry resembles that taken by CVB3 (10), although unlike the case for CVB3, no binding partner for EV11-207 has been identified in tight junctions to date. In contrast, EV11-207R appears to enter directly at the apical surface of cells, fails to alter tight junction permeability, and thus resembles the non-DAF/CD55-binding coxsackievirus strain CVB3-Nancy. Replication of this virus proceeds with similar kinetics to those of EV11-207 (data not shown). In addition to EV11-207 and coxsackie B viruses, adenoviruses, reoviruses, certain herpesviruses, and hepatitis C virus have also been shown to transit through tight junctions or to use tight junction proteins for infection (5, 10, 15). Since virus mutants that do not enter through tight junctions can also infect cells *in vitro*, it is not clear what advantages entry through tight junctions offers to viruses such as EV11-207, though this entry route may be more relevant *in vivo*, where

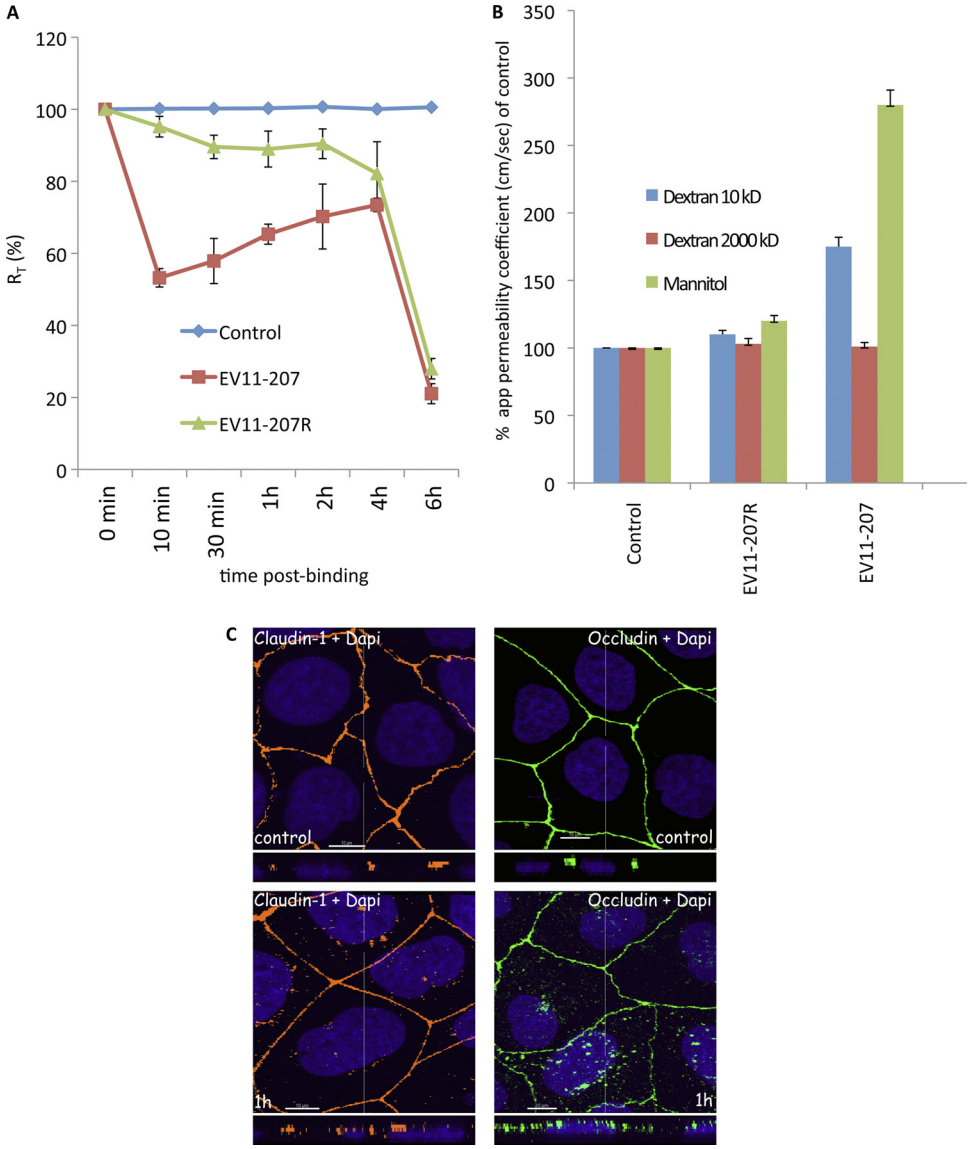

FIG. 8. EV11-207 entry leads to a decrease of transepithelial resistance (R_T) and an increase of the paracellular permeability of Caco-2 monolayers. (A) Caco-2 monolayers grown on Transwell membranes were left untreated (control) or exposed to EV11-207 or EV11-207R (100 PFU/cell) at 4°C for 30 min to allow virus attachment. The cells were washed (0 min) and warmed to 37°C. R_T was measured at the indicated time points. Data are means ± SD for 7 monolayers. (B) Caco-2 monolayers grown on Transwell membranes were exposed or not (control) to EV11-207 or EV11-207R (100 PFU/cell) at 4°C for 30 min to allow virus attachment. The cells were washed, and [^{3}H]dextrans or [^{14}C]mannitol was added at the apical surface. Cells were warmed to 37°C for 1 h, and flux (apical to basal) of dextrans or mannitol was measured. Results are expressed as apparent permeability coefficients (app) (means plus SD) for 4 monolayers. (C) Claudin-1 and occludin are displaced out of tight junctions. Polarized Caco-2 monolayers were fixed (control) or exposed to EV11-207 (100 PFU/cell) at 4°C for 30 min to allow virus attachment. The cells were washed, warmed to 37°C for 1 h, and then fixed. Cells were permeabilized and stained with anti-claudin-1 MAb (yellow) or anti-occludin MAb (green) and DAPI (blue). Bars = 10 μm.

the harsh environment present in the intestinal lumen may select against direct virus entry, perhaps through effects on uncoating intermediates. The advantage to EV11-207 of transit through tight junctions remains to be elucidated. The present data reinforce the notion that picornaviruses exhibit a broad range of genetic variations and phenotypic plasticities (3, 26, 35, 49). As a result, picornaviruses are capable of exploiting multiple adaptive solutions that are not correlated with evolutionary history (31).

As with other infectious agents, the passage of EV11-207 through tight junctions affects their structure and function. The loss of transepithelial resistance seen 10 min after the initiation of virus infection begins to be restored by cells within 30 min after infection. This is the time point at which we observed displacement of some proteins, such as occludin and claudin-1 (Fig. 8C), from the tight junctions. Since no binding partner of EV11-207 is known to reside in or play a role in junction integrity, the loss of transepithelial resistance and concomitant increase of monolayer permeability could result from the movement of the junction proteins. Indeed, numerous studies

have reported the internalization of tight junction proteins in association with the loss of tight junction integrity (7, 9, 16, 23, 24, 51, 52, 55).

In contrast to observations made with coxsackie B virus (12), no intracellular colocalization of EV11-207 with occludin could be detected. Thus, while EV11-207 and CVB3 use superficially similar routes of entry, the details appear to differ. CVB3 uses coxsackie and adenovirus receptor (CAR) as its cellular receptor, while the receptor involved in EV11-207 uncoating remains unknown. In addition, by use of an unknown transmembrane coupling mechanism, DAF clustering induced by CVB3 activates cytosolic nonreceptor tyrosine kinases, such as Abl, Fyn, and Src, and activates actin remodeling. This allows CVB3 to target the tight junction protein CAR, which triggers conformational changes in the viral capsid necessary for subsequent genome release upon endocytosis (10, 17). Thus, the initial stages of CVB3 uncoating appear to occur at the cell surface. In this respect, CVB3 entry appears to resemble poliovirus entry (6, 11). In contrast, the observation that DAF remains associated with EV11-207 during the entry process, along with our previous data obtained with nonpolarized cells, suggests that EV11-207 remains intact throughout the process of endocytosis and that uncoating and genome release occur in an intracellular compartment, probably the recycling endosome (46). The cell biology of picornavirus uncoating remains poorly understood (10). Further studies will be required to decipher the mechanisms underlying this entry pathway and other factors required for EV11-207 uncoating.

In conclusion, we demonstrate here that at least two different entry routes (one via tight junctions and the other directly from the apical surface) can be employed by echovirus 11 during infection of polarized epithelial cells, with DAF binding at the apical surface being a critical determinant. While cholesterol depletion inhibits infection by EV11-207 by leading to DAF aggregation, and presumably internalization, only minor effects are observed on DAF-independent direct internalization of mutant viruses through the apical surface. Work is in progress to look at signaling events during EV11 entry.

ACKNOWLEDGMENTS

D. Nkwe and A. Pelchen-Matthews are acknowledged for their critical readings of the initial manuscript. Mark Marsh is warmly acknowledged for fruitful discussions. We are grateful to Gisou F. van der Goot for providing an EVOM ohmmeter.

This work was supported by grants from the Swiss National Science Foundation to T.A.M. and K.S. and by UK Medical Research Council funding to the Cell Biology Unit, MRC Laboratory for Molecular Cell Biology, University College London.

REFERENCES

1. **Abrami, L., S. Liu, P. Cosson, S. H. Leppla, and F. G. van der Goot.** 2003. Anthrax toxin triggers endocytosis of its receptor via a lipid raft-mediated clathrin-dependent process. J. Cell Biol. **160:**321–328.
2. **Abrami, L., and F. G. van Der Goot.** 1999. Plasma membrane microdomains act as concentration platforms to facilitate intoxication by aerolysin. J. Cell Biol. **147:**175–184.
3. **Agol, V. I.** 2001. Translational control of the picornavirus phenotype. Mol. Biol. **35:**591–599.
4. **Babbin, B. A., M. Sasaki, K. W. Gerner-Schmidt, A. Nusrat, and J. M. Klapproth.** 2009. The bacterial virulence factor lymphostatin compromises intestinal epithelial barrier function by modulating rho GTPases. Am. J. Pathol. **174:**1347–1357.
5. **Barton, E. S., et al.** 2001. Junction adhesion molecule is a receptor for reovirus. Cell **104:**441–451.
6. **Brandenburg, B., et al.** 2007. Imaging poliovirus entry in live cells. PLoS Biol. **5:**e183.
7. **Bruewer, M., S. Samarin, and A. Nusrat.** 2006. Inflammatory bowel disease and the apical junctional complex. Ann. N. Y. Acad. Sci. **1072:**242–252.
8. **Cakebread, J. A., et al.** 2011. Exogenous IFN-beta has antiviral and anti-inflammatory properties in primary bronchial epithelial cells from asthmatic subjects exposed to rhinovirus. J. Allergy Clin. Immunol. **127:**1148–1154.
9. **Capaldo, C. T., and A. Nusrat.** 2009. Cytokine regulation of tight junctions. Biochim. Biophys. Acta **1788:**864–871.
10. **Coyne, C. B., and J. M. Bergelson.** 2006. Virus-induced Abl and Fyn kinase signals permit coxsackievirus entry through epithelial tight junctions. Cell **124:**119–131.
11. **Coyne, C. B., K. S. Kim, and J. M. Bergelson.** 2007. Poliovirus entry into human brain microvascular cells requires receptor-induced activation of SHP-2. EMBO J. **26:**4016–4028.
12. **Coyne, C. B., L. Shen, J. R. Turner, and J. M. Bergelson.** 2007. Coxsackievirus entry across epithelial tight junctions requires occludin and the small GTPases Rab34 and Rab5. Cell Host Microbe **2:**181–192.
13. **Dandekar, S., M. D. George, and A. J. Baumler.** 2010. Th17 cells, HIV and the gut mucosal barrier. Curr. Opin. HIV AIDS **5:**173–178.
14. **Fukayama, M.** 2010. Epstein-Barr virus and gastric carcinoma. Pathol. Int. **60:**337–350.
15. **Geraghty, R. J., C. Krummenacher, G. H. Cohen, R. J. Eisenberg, and P. G. Spear.** 1998. Entry of alphaherpesviruses mediated by poliovirus receptor-related protein 1 and poliovirus receptor. Science **280:**1618–1620.
16. **Gill, R. K., et al.** 2008. Serotonin modifies cytoskeleton and brush-border membrane architecture in human intestinal epithelial cells. Am. J. Physiol. Gastrointest. Liver Physiol. **295:**G700–G708.
17. **Greber, U. F., and M. Gastaldelli.** 2007. Junctional gating: the Achilles' heel of epithelial cells in pathogen infection. Cell Host Microbe **2:**143–146.
18. **Harhaj, N. S., and D. A. Antonetti.** 2004. Regulation of tight junctions and loss of barrier function in pathophysiology. Int. J. Biochem. Cell Biol. **36:** 1206–1237.
19. **Hartsock, A., and W. J. Nelson.** 2008. Adherens and tight junctions: structure, function and connections to the actin cytoskeleton. Biochim. Biophys. Acta **1778:**660–669.
20. **Hutt-Fletcher, L. M., and L. S. Chesnokova.** 2010. Integrins as triggers of Epstein-Barr virus fusion and epithelial cell infection. Virulence **1:**395–398.
21. **Itoh, M., and M. J. Bissell.** 2003. The organization of tight junctions in epithelia: implications for mammary gland biology and breast tumorigenesis. J. Mammary Gland Biol. Neoplasia **8:**449–462.
22. **Ivanov, A. I.** 2008. Actin motors that drive formation and disassembly of epithelial apical junctions. Front. Biosci. **13:**6662–6681.
23. **Ivanov, A. I., A. Nusrat, and C. A. Parkos.** 2004. Endocytosis of epithelial apical junctional proteins by a clathrin-mediated pathway into a unique storage compartment. Mol. Biol. Cell **15:**176–188.
24. **Ivanov, A. I., A. Nusrat, and C. A. Parkos.** 2004. The epithelium in inflammatory bowel disease: potential role of endocytosis of junctional proteins in barrier disruption. Novartis Found. Symp. **263:**115–124.
25. **Kawaguchi, H., Y. Akazawa, Y. Watanabe, and Y. Takakura.** 2005. Permeability modulation of human intestinal Caco-2 cell monolayers by interferons. Eur. J. Pharm. Biopharm. **59:**45–50.
26. **Kilpatrick, D. R., J. Quay, M. A. Pallansch, and M. S. Oberste.** 2001. Type-specific detection of echovirus 30 isolates using degenerate reverse transcriptase PCR primers. J. Clin. Microbiol. **39:**1299–1302.
27. **Lafont, F., G. Tran Van Nhieu, K. Hanada, P. Sansonetti, and F. G. van der Goot.** 2002. Initial steps of Shigella infection depend on the cholesterol/sphingolipid raft-mediated CD44-IpaB interaction. EMBO J. **21:**4449–4457.
28. **Landmann, L., and P. Marbet.** 2004. Colocalization analysis yields superior results after image restoration. Microsc. Res. Tech. **64:**103–112.
29. **Lea, S. M., et al.** 1998. Determination of the affinity and kinetic constants for the interaction between the human virus echovirus 11 and its cellular receptor, CD55. J. Biol. Chem. **273:**30443–30447.
30. **Lewis, S. A., J. R. Berg, and T. J. Kleine.** 1995. Modulation of epithelial permeability by extracellular macromolecules. Physiol. Rev. **75:**561–589.
31. **Lewis-Rogers, N., and K. A. Crandall.** 2010. Evolution of Picornaviridae: an examination of phylogenetic relationships and cophylogeny. Mol. Phylogenet. Evol. **54:**995–1005.
32. **Lu, S., A. W. Gough, W. F. Bobrowski, and B. H. Stewart.** 1996. Transport properties are not altered across Caco-2 cells with heightened TEER despite underlying physiological and ultrastructural changes. J. Pharm. Sci. **85:**270–273.
33. **Manders, E. M. M., F. J. Verbeek, and J. A. Aten.** 1993. Measurement of colocalization of objects in dual-color confocal images. J. Microsc. (Oxford) **169:**375–382.
34. **Nikolic, D., Y. Li, L. R. Chadwick, and R. B. van Breemen.** 2006. In vitro studies of intestinal permeability and hepatic and intestinal metabolism of 8-prenylnaringenin, a potent phytoestrogen from hops (Humulus lupulus L.). Pharm. Res. **23:**864–872.
35. **Oberste, M., D. Schnurr, K. Maher, S. al-Busaidy, and M. Pallansch.** 2001. Molecular identification of new picornaviruses and characterization of a proposed enterovirus 73 serotype. J. Gen. Virol. **82:**409–416.
36. **Patel, J. R., J. Daniel, and V. I. Mathan.** 1985. An epidemic of acute

diarrhoea in rural southern India associated with echovirus type 11 infection. J. Hyg. (London) **95:**483–492.
37. **Pettigrew, D. M., et al.** 2006. Structural and functional insights into the interaction of echoviruses and decay-accelerating factor. J. Biol. Chem. **281:** 5169–5177.
38. **Plevka, P., et al.** 2010. Interaction of decay-accelerating factor with echovirus 7. J. Virol. **84:**12665–12674.
39. **Powell, R., T. Ward, D. Evans, and J. Almond.** 1997. Interaction between echovirus 7 and its receptor, decay-accelerating factor (CD55): evidence for a secondary cellular factor in A-particle formation. J. Virol. **71:**9306–9312.
40. **Renois, F., et al.** 2011. Development of a recombinant CHO cell model for the investigation of CAR and DAF role during early steps of echovirus 6 infection. Virus Res. **158:**46–54.
41. **Revello, M. G., and G. Gerna.** 2010. Human cytomegalovirus tropism for endothelial/epithelial cells: scientific background and clinical implications. Rev. Med. Virol. **20:**136–155.
42. **Rodenhuis-Zybert, I. A., J. Wilschut, and J. M. Smit.** 2010. Dengue virus life cycle: viral and host factors modulating infectivity. Cell. Mol. Life Sci. **67:** 2773–2786.
43. **Samarin, S., and A. Nusrat.** 2009. Regulation of epithelial apical junctional complex by Rho family GTPases. Front. Biosci. **14:**1129–1142.
44. **Sanders, C. J., P. C. Doherty, and P. G. Thomas.** 2011. Respiratory epithelial cells in innate immunity to influenza virus infection. Cell Tissue Res. **343:** 13–21.
45. **Schneeberger, E. E., and R. D. Lynch.** 2004. The tight junction: a multifunctional complex. Am. J. Physiol. Cell Physiol. **286:**C1213–C1228.
46. **Stuart, A. D., H. E. Eustace, T. A. McKee, and T. D. Brown.** 2002. A novel cell entry pathway for a DAF-using human enterovirus is dependent on lipid rafts. J. Virol. **76:**9307–9322.
47. **Stuart, A. D., et al.** 2002. Determination of the structure of a decay accelerating factor-binding clinical isolate of echovirus 11 allows mapping of mutants with altered receptor requirements for infection. J. Virol. **76:**7694–7704.
48. **Stutts, M. J., R. C. Boucher, P. A. Bromberg, and J. T. Gatzy.** 1981. Effects of ammonium and nitrate salts on lon transport across the excised canine trachea. Toxicol. Appl. Pharmacol. **60:**91–105.
49. **Svitkin, Y. V., N. Cammack, P. D. Minor, and J. W. Almond.** 1990. Translation deficiency of the Sabin type 3 poliovirus genome: association with an attenuating mutation C472—-U. Virology **175:**103–109.
50. **Tsukita, S., M. Furuse, and M. Itoh.** 2001. Multifunctional strands in tight junctions. Nat. Rev. Mol. Cell. Biol. **2:**285–293.
51. **Turner, J. R.** 2006. Molecular basis of epithelial barrier regulation: from basic mechanisms to clinical application. Am. J. Pathol. **169:**1901–1909.
52. **Utech, M., et al.** 2005. Mechanism of IFN-γ-induced endocytosis of tight junction proteins: myosin II-dependent vacuolarization of the apical plasma membrane. Mol. Biol. Cell **16:**5040–5052.
53. **Vareille, M., E. Kieninger, M. R. Edwards, and N. Regamey.** 2011. The airway epithelium: soldier in the fight against respiratory viruses. Clin. Microbiol. Rev. **24:**210–229.
54. **Walsh, S. V., A. M. Hopkins, and A. Nusrat.** 2000. Modulation of tight junction structure and function by cytokines. Adv. Drug Deliv. Rev. **41:**303–313.
55. **Yu, D., and J. R. Turner.** 2008. Stimulus-induced reorganization of tight junction structure: the role of membrane traffic. Biochim. Biophys. Acta **1778:**709–716.
56. **Zinchuk, V., O. Zinchuk, and T. Okada.** 2007. Quantitative colocalization analysis of multicolor confocal immunofluorescence microscopy images: pushing pixels to explore biological phenomena. Acta Histochem. Cytochem. **40:**101–111.